



Published in final edited form as:

*J Biomech Eng.* 2008 April ; 130(2): 021006. doi:10.1115/1.2898716.

## Continuum mechanics analysis of fracture progression in the vitrified cryoprotective agent DP6

Paul S. Steif, Matthew C. Palastro, and Yoed Rabin<sup>1</sup>

*Biothermal Technology Laboratory Department of Mechanical Engineering Carnegie Mellon University 5000 Forbes Avenue, Pittsburgh, PA 15237*

### Abstract

As part of an ongoing effort to study the continuum mechanics effects associated with cryopreservation, the current report focuses on the prediction of fracture formation in cryoprotective agents. Fractures had been previously observed in 1 ml samples of the cryoprotective agent cocktail DP6, contained in a standard 15 ml glass vial, and subjected to various cooling rates. These experimental observations were obtained by means of a cryomicroscope, which has been recently presented by the current research team. High and low cooling rates were found to produce very distinct patterns of cracking. The current study seeks to explain the observed patterns on the basis of stresses predicted from finite element analysis, which relies on a simple viscoelastic constitutive model and on estimates of the critical stress for cracking. The current study demonstrates that the stress which results in instantaneous fracture at low cooling rates is consistent with the stress to initiate fracture at high cooling rate. This consistency supports the credibility of the proposed constitutive model and analysis, and the unified criterion for fracturing, that is, a critical stress threshold.

### Keywords

Cryomicroscopy; vitrification; continuum mechanics; fracture; DP6

### Introduction

One of the many factors that impact the survival and integrity of living biological tissues post cryopreservation is the development of thermo-mechanical stress during the cryogenic process [1-4] (or “thermal stress”). Fracture formation is probably the most dramatic outcome of thermal stress, and it is a limiting factor that prevents the widespread application of cryopreservation technology to bulky tissues and organs [1,3,5-7]. Thermal stress is driven by the phenomenon of thermal expansion, which has been studied intensively in recent years in the context of cryobiology [8-14]. In order to increase cell survival, cryopreservation is most frequently conducted with the addition of cryoprotective agents (CPA), which affect the kinetics of solidification. The CPA reduces, and possibly circumvents ice crystal formation, which is destructive to biological cells. Crystallization can be prevented completely at high cooling rates or at high cryoprotectant concentrations, where the CPA becomes vitrified (vitreous in Latin means glass). While complete vitrification can potentially prevent the devastating effect of ice crystallization [15], the high concentration of the CPA involved in it is potentially very toxic [2,16-19].

<sup>1</sup>Corresponding author; Phone: (412) 268 2204; Fax: (412) 268 3348; Email: Rabin@CMU.EDU

The study of thermal stress effects in cryobiology can be classified with respect to the process of freezing: crystallization, vitrification, or a combination of both. Mathematical modeling of thermal stress during crystallization, in the absence of CPAs, is the least complex [20,21]. The material is most conveniently subdivided into regions according to the phase of state. The frozen material is typically assumed to behave like a linear-elastic material, having a linear relationship between strain and stress; the unfrozen material is assumed to behave like a stationary liquid, incapable of supporting shear stress. Additional model assumptions must be made when phase transition occurs over a temperature range, which is typically the case in biological materials. However, experimental evidence on the mechanical behavior of the material in the phase transition temperature range is largely unknown.

While the mathematical modeling of thermal stress during vitrification is largely uncharted, concepts from the general field of continuum mechanics clearly must be drawn upon. Analysis must account for the elevation of the viscosity by fourteen orders of magnitude, associated with cooling the material from room temperature to the so-called glass transition temperature [14,22]; this dramatic property change produces a continuous transformation from a liquid-like material to a solid-like material. Stresses in a vitrified material would produce both elastic (instantaneous) deformation, as well as “creep” or viscous deformation. In creep, the strain increases continually under constant stress, where the creep strain rate is inversely proportional to the viscosity. Creep strain dominates elastic strains at higher temperatures; with a decrease in temperature, the elastic strain becomes comparable to, and eventually dominates, the creep strain. A “set temperature” below which the vitrified material is predicted to behave elastically has been recently proposed in the context of cryobiology [22].

Cryopreservation, subject to a low concentration CPA and sub-critical cooling rates to promote vitrification, is widely known as classical cryopreservation. In classical cryopreservation, ice crystals first nucleate at about the heterogeneous nucleation point for the specific cryoprotectant composition, while the concentration of the remaining solution elevates. The progress of crystal formation, and elevation of the concentration of the remaining solution, continues with cooling, until the remaining solution becomes so viscous as to form glass at the particular cooling rate [8]. One could view classical preservation as localized vitrification in small regions, or “pockets”. The volume fraction eventually occupied by ice crystals is affected by many factors, and the coexistence of crystallized and vitrified regions is an inevitable outcome of classical cryopreservation. Modeling of classical cryopreservation is a very challenging task; the formation of pockets of vitrified material can only be modeled statistically and is difficult to predict. It seems that continuum mechanics effects associated with classical cryopreservation can be modeled only after cryopreservation by vitrification alone is better understood in the continuum mechanics sense. Many continuum mechanics effects in the vitrification of biomaterials are presently unexplored.

In order to study critical cooling rates for vitrification of various CPAs, a new device has been developed recently, termed a “cryomicroscope” [6]. The microscope enables video recording of the cooled material in standard vials, for identification of crystallization and vitrification events on the macro-scale. As a byproduct of the CPA cooling process, fractures were observed using the cryomicroscope [7]. These fractures were primarily radial; they occurred instantaneously throughout the vial at slow cooling rates, while they gradually progressed inwards in high cooling rates. The current study is aimed at providing a plausible explanation for these patterns of cracking.

The current report starts with a brief review of the experimental system used to observe fracture formation in a CPA contained in a vial. Next, two representative sets of results of cracking in the CPA cocktail DP6 are presented; one at low and the other at high cooling rates. A mathematical formulation of the stress problem is proposed, and solved using the commercial

code ANSYS. Patterns of cracking are then predicted by combining the calculated stresses with critical levels of stress for fracture that were inferred from experimental observations of cracking in thin films [22]. While the observations of cracking and the viscoelastic constitutive law used to analyze the cracking have been presented previously by the authors, the unique contribution of the current study is to use calculations of stress to predict the temperature at which cracking should occur under conditions of non-uniform temperature. In doing so, this study demonstrates that very different patterns of progressive cracking at fast and slow cooling rates are, in fact, consistent with a single cracking criterion, that is, a critical stress to fracture.

## Experimental Setup and Observations

The experimental setup is presented in detail in [6], and is described here in brief, for completeness of presentation. The macroscope, Fig. 1, is constructed of four main components: a Hyper HAD CCD camera (SI-M350, Costar, Inc.), a borescope (HH12-AF, Gradient Lens Corporation, Inc.), a standard vial, and a cooling chamber. A 15 ml glass vial, containing 1 ml of CPA, is connected to the tip of the borescope with a special adapter (the inner diameter of the vial is 25 mm and the height of the CPA is about 2 mm). Through the adapter, a thermocouple is extended into the vial, where the thermocouple junction is placed at the center of the CPA by means of a plastic guide (tube). As discussed in [6], the typical resolution for the particular setup is 15  $\mu\text{m}$  at the bottom of the vial.

Video recording and temperature monitoring is performed simultaneously throughout the experiment. The CPA is initially at room temperature. The experiment starts with lowering the assembly of the camera, borescope, and vial, along the pole (illustrated in Fig. 1), into a top-open air chamber, which is surrounded by a cylindrical liquid nitrogen container. Heat transfer by free convection prevails in the air, between the vial and the liquid nitrogen. In order to passively control the cooling rate of the vial, a thermal insulation sleeve (delrin) covers the glass vial. The thermal sleeve behaves as a thermal insulator, reducing the rate of heat transfer from the vial. In practice, a series of thermal sleeves is used to generate a range of cooling rates, where a thicker sleeve leads to lower cooling rates.

The technique of cooling a sample by free convection is common practice in cryopreservation, when slow to moderate cooling rates are required. Most frequently, this is done within standard liquid nitrogen containers, where the sample is kept above the liquid surface, in the nitrogen vapor phase. By adjusting the height of the sample from the liquid surface, the minimum cryogenic temperature is controlled, as well as the maximum cooling rate.

A wide range of experimental conditions is reported in [6,7], from which two typical experiments were selected for the current analysis, representing low and high cooling rates. These experiments were performed on DP6, which is a cocktail of 234.4 g/l DMSO (3M), 228.3 g/l propylene glycol (3M), and 2.4 g/l HEPES in a EuroCollins solution. [9,13].

With reference to Fig. 2, the top two images display representative results from a slow cooling rate experiment. The cryoprotectant can be seen before (top-left) and after (top-right) cracking, which occurs when the temperature at the center of the cryoprotectant is  $-127.2^{\circ}\text{C}$ ; the time difference between the two images is one frame at a speed of 15 frames per second. The printed polar grid of radial and circumferential lines seen in this figure serves as a reference for length measurements; this grid is placed between the vial and the thermal insulation sleeve. The bright area at the center of each image represents a reflection of light [23]; one difficulty in using a borescope for the current study is that the light source and the optical device are parallel to one another, and the studied substance is in its glassy state. The lower two images display representative results from a fast cooling experiment, when the temperature at the center of the cryoprotectant reaches  $-129.8^{\circ}\text{C}$  (bottom-left) and  $-156.4^{\circ}\text{C}$  (bottom-right). A clear

progression of a cracking front is observed in the fast cooling rate experiment, where the bottom-right image in Fig. 2 corresponds to the instant where this front reaches the center of the vial. More images on fracture formation CPAs in vials are available at [5], and fracture formation in thin films of the same CPAs at [23].

## Mathematical Formulation

It is assumed that flow, deformation, and stress have negligible effect on temperatures. Hence, the heat transfer problem is solved first, and its results serve as input to the calculations of stress. A schematic illustration of the mathematical problem is shown in Fig. 1(b), which is assumed to be axi-symmetric.

The formulation of the heat transfer problem assumes pure conduction everywhere in the domain, including the CPA. The initial condition is of a uniform temperature of 20°C (room temperature). A convective boundary condition, subject to a constant heat transfer coefficient, is assumed between the vial and the liquid nitrogen container (−196°C), through the base and the side wall. Consistent with the analysis in [7], the value of the heat transfer coefficient by convection has been determined using an inverse analysis, to best fit experimental temperature measurements with simulation results at the center of the vial (at the location of the thermocouple, Fig. 1(c)). Finally, since heat transfer to the air contained in the vial was deemed negligible, and since the vial is tall compared with the wall thickness (a ratio greater than 20:1), a condition of zero heat flux (mathematical insulation) was assumed on the remaining boundary, Fig. 1(b).

The formulation of the continuum mechanics problem assumes viscoelastic behavior for the CPA, and linear-elastic behavior for the glass vial and the delrin sleeve. As discussed in [7], the stress response of the CPA in uniaxial tension is modeled with a simple viscoelastic law:

$$\dot{\epsilon} = \frac{1}{E_{CPA}} \frac{d\sigma}{dt} + \frac{\sigma}{3\eta} + \beta_{CPA} \frac{dT}{dt} \quad (1)$$

where  $\delta$  is the stress,  $E_{CPA}$  is the Young's modulus,  $\eta$  is the shear viscosity, and  $\beta_{CPA}$  is the coefficient of thermal expansion. That model describes the total strain-rate,  $\dot{\epsilon}$ , as the linear superposition of (from left in Eq. (1)) the elastic strain-rate, the viscous (or creep) strain-rate, and the thermal strain-rate [24]. Equation (3) in [7] was based on the same uniaxial behavior as Eq. (1) in the present paper; in [7] it was applied to the case of equal biaxial tension assuming the uniaxial behavior generalizes isotropically. The FEA models to be used here also assume isotropic response, but allow for more general (axisymmetric) stress states. The temperature-dependent terms in Eq. (1) utilize the solution of the heat transfer problem solved previously. Note that stresses are computed in the CPA assuming that cracks are absent; accounting for the effects of accumulating cracks, given the complexity of the viscoelastic law and varying temperatures, is beyond the scope of the current investigation. Due to the tolerance between the thermal sleeve and the vial, the sleeve's resistance to deformation is neglected; hence, boundary conditions of zero normal and shear stresses on the outer surfaces of CPA and vial were assumed.

## Material Properties and Computation Parameters

The material properties used in this study are listed in Table 1. For the CPA, the dependency of the thermal conductivity on temperature is largely unknown. Since DP6 is a water-based solution, and since the thermal conductivity of water increases exponentially with decreasing temperature [25], a similar dependency was assumed for the DP6 cocktail, with the only exception that the reference value at 273K is shifted down to 0.2 W/m-K. The 0.2 value corresponds to 7.05M DMSO, which has similar mass of solutes as of DP6; DMSO is a key ingredient in DP6, and the only ingredient for which thermal conductivity data is available

[26]. Based on the similarity of its constituents, the density of the CPA is taken to be the same as the density of 7.05M DMSO at room temperature [7,27], and its temperature dependency is compiled from [9]. The specific heat of the DP6 is unknown; from arguments similar to those presented above, a representative specific heat of 7.05M DMSO at room temperature is taken, where its linear dependency is compiled from [28]. The Poisson ratio selected for the CPA is typical of brittle materials [29], and the elasticity modulus is typical of organic materials [30]; both are independent of temperature. As discussed in [22], the results were found to be insensitive to the precise values chosen. The corresponding properties for glass and delrin were assumed to be temperature independent, with average values from the literature.

The viscosity of DMSO at various molar concentrations has been measured in the temperature range of 20°C –45°C with falling ball viscometry [27]; the authors are unaware of viscosity measurements of DMSO at lower temperatures, or of DP6 at all. The viscosity of DMSO in the temperature range of interest (in the vicinity of glass transition) is orders of magnitude higher than that in the range of available experimental data [27]. While the glass transition temperature,  $T_g$ , is commonly measured with differential calorimetry techniques (DSC), an alternative definition of glass transition is the temperature at which the viscosity reaches  $10^{12}$  Pa-s ( $10^{13}$  Poise). In the absence of viscosity data at low temperatures, the following functional behavior is assumed [27]:

$$\eta(T) = \eta_0 \exp\left(\frac{b}{T - T_0}\right) \quad [Pa - s] \quad ; \quad \eta_0 = 10^{12} \exp\left(\frac{-b}{T_g - T_0}\right) \quad (2)$$

where parameters  $T_0 = 132.2$  K and  $b = 5.45$  K<sup>-1</sup> are chosen to fit the available experimental data for DMSO at higher temperatures [22]. Equation (2) yields a viscosity value of  $10^{12}$  Pa-s at the glass transition temperature (-119°C, measured with DSC [6]).

The heat transfer coefficient by convection,  $h$ , was found by means of inverse analysis [7]. In brief, the heat transfer simulation was performed many times with different  $h$  values, using the material properties presented above, until the experimental temperature data obtained at the center of the vial best-fitted the simulation results (see, for example, Fig. 3). Best-fit values of 55 W/m<sup>2</sup>-C and 350 W/m<sup>2</sup>-C were found for the slow and fast cooling rates, respectively.

Both heat transfer and stress analysis were carried out using ANSYS 8.1. In the CPA, there were 403 eight-noded axisymmetric elements of type Plane77 for the heat transfer simulation, and 403 eight-noded axisymmetric elements of type Plane183 for the stress analysis. Special steps were taken due to the fact that the viscosity varies over many orders of magnitude within the simulated temperature range. During initial cooling from room temperature, when the viscosity is low, impractically small time steps would be required to ensure stability of simulation (on the order of  $10^{-10}$  s). Likewise, the viscosity function well below glass transition is clearly incorrect. To overcome these problems, a piecewise viscosity function is assumed, where the viscosity is represented by Eq. (2) in the temperature range corresponding to the viscosity values of  $3 \times 10^8$  Pa-s to  $10^{20}$  Pa-s; the viscosity remains constant at a value of  $3 \times 10^8$  Pa-s at higher temperatures, and constant at a value of  $10^{20}$  Pa-s at lower temperatures. This simplification leads to higher predicted stress at high temperatures; however, the stress level even with the artificially high values of viscosity is still orders of magnitude lower than the stress level associated with cracking. At low temperatures on the other hand, the viscosity value is so high that material response is virtually elastic; the effect of limiting the viscosity value to  $10^{20}$  Pa-s is, therefore, negligible.

## Results and Discussion

The fundamental mechanism of stress development in the experiments of interest has been presented in [7,22]. In brief, the CPA has a coefficient of thermal expansion that is much higher

than that of the vial. Consequently, the CPA shrinks with cooling at a greater rate than the vial. The vial, being much stiffer than the CPA, prevents the CPA from shrinking by applying stresses to it. When the temperature is high and the viscosity of CPA is low, the CPA can deform easily in response to the difference in material shrinkage; this results in relatively low stresses in the CPA. As the temperature is reduced and the CPA viscosity rises, the CPA flows more slowly and gradually comes to respond like an elastic solid (i.e., stresses become proportional to the shrinkage difference between CPA and vial). Eventually the stresses exceed the strength of the CPA and produce cracks.

The temperature distribution in the CPA is presented in Fig. 4, at three instants in time, for the cases of fast and slow cooling rates. Each pair (row) of plots corresponds to the same temperature at the geometric center of the CPA,  $T_c$ . It can be seen that the temperature variation is primarily in the radial direction, although moderate temperature variation also exists in the axial direction within the CPA layer. As expected, the temperature distribution is far less uniform in the high cooling rate case, when compared with the low cooling rate case. The temperature distribution is seen to become more uniform at lower temperatures for either case, reflecting the increase of thermal conductivity with cooling.

Predictions of the circumferential stress, for the corresponding instants in time, are presented in Fig. 5. The circumferential stress is somewhat greater than the radial stress that acts in the plane of the layer (not shown); the shear stresses are significantly lower. The case of slow cooling exhibits nearly uniform stresses, consistent with the temperature field. A model for calculating the stress in a thin circular droplet of CPA on a substrate, based on uniform temperature and a simple uniform stress field [22], yields predictions of stress that are nearly equivalent to those found for the slow cooling case. By contrast, the stresses vary with position significantly for the fast cooling case. Thus, the stresses in the outer portion of the vial could reach the fracture stress much earlier than those in the center during fast cooling. Predictions of stress are less reliable in the outermost portions of vial due to uncertainties in boundary conditions, such as the precise shape of the vial, and possibly surface tension effects in the CPA. Note that all stress values are positive, representing tensile stress. Brittle materials are much more susceptible to fracture in tension than compression. Below, cracking will be assumed to occur at some point upon reaching a critical tensile stress. Since the shear stress and the normal stress through the thickness are small compared to the circumferential stress, the maximum tensile stress is essentially equal to the circumferential stress, which is the only stress component displayed in this report.

The variation of the circumferential stress with radial position, for the top and bottom surfaces of the CPA, is shown in Fig. 6 for (a)  $T_c = -120^\circ\text{C}$  and (b)  $T_c = -130^\circ\text{C}$ ; it can be seen that the stresses are more uniform at lower temperatures. At  $T_c = -130^\circ\text{C}$ , the circumferential stress at the center reaches the value 1.8 MPa, which was the fracture stress inferred for DP6 in an earlier study, in which a thin film of DP6 was vitrified on a copper plate [22]. (Higher stresses are predicted at the vial wall, but these stresses are strongly dependent on end effects, which are not deemed to be captured adequately in the current study.) For the slow cooling of the CPA in vials, different experiments exhibited cracking simultaneously through the CPA when the center temperature ranged from  $T_c = -127^\circ\text{C}$  to  $T_c = -130^\circ\text{C}$ . Circumferential stresses at the center are predicted to be from 1.5 MPa to 1.8 MPa over this temperature range.

From Fig 6(a), one can see that the stresses are below 1.8 MPa for the case of slow cooling rate at  $T_c = -120^\circ\text{C}$ . In the fast cooling case, however, this stress is exceeded for the same center temperature, in the outer portion of the vial (approximately in  $0.4 < r/R < 1$ ). Thus, one would suspect that conditions for cracking are exceeded at radii greater than  $r/R=0.4$  in the CPA. As pointed out above, this method of inferring the extent of cracking is based purely on the stresses calculated under the assumption of no cracks; the formation of a crack is expected

to relieve some of the stress in its vicinity. Thus, the stress distribution computed in this study represents an upper bound for stress development during crack formation. Nevertheless, using this approach, the extent of cracking in the fast cooling case can be predicted for each instant in time. Figure 7 presents the predicted and observed cracking front as functions of  $T_c$ . Cracks are first observed to appear fully formed, occupying the region  $0.8 < r/R < 1$ , and then to progress gradually towards the center. Computational predictions follow the same general trend as the experimental observations, although cracks do not appear to reach the center until a temperature  $18^\circ\text{C}$  below the predicted value. Again, one must bear in mind that stresses are predicted based on ignoring the presence of cracks. Furthermore, progression of cracking in conventional materials is often predicted using the more complex methodology of fracture mechanics; this approach was not pursued here, given the significant uncertainties in material properties.

## Summary and Conclusions

Previous work has shown that cracking in cryoprotective agents at low temperatures can be explained on the basis of thermo-mechanical stresses. The current study focuses on a theoretical analysis of previously reported experimental observations of fracture formation in the cryoprotectant cocktail DP6, contained in a glass vial, and subjected to different cooling conditions. It was observed that slow cooling rate experiments resulted in cracks initiating throughout the CPA, while fast cooling rate experiments resulted in cracks initiating in the outer (colder) region, while the center temperature is still relatively warm; cracks subsequently propagated into the inner region as it becomes colder. The current study utilizes data on tensile fracture stress from a second experimental study, where a value of 1.8 MPa was inferred for DP6.

In the current study, calculations of temperatures and the resulting stresses were undertaken using finite element analysis, with the commercial code ANSYS. Good agreement was obtained between predicted and measured temperatures at which cracking occurs in the slow cooling case, and at which cracking initiates in the fast cooling case. The current study demonstrates that the stress that results in instantaneous fracturing at low cooling rates is consistent with the stress for the onset of fracture at high cooling rate. This consistency supports the credibility of the proposed constitutive model and analysis, and the unified criterion for fracturing, that is, a critical stress threshold. Inward progression of cracks in the fast cooling case is predicted to occur more rapidly than is observed. The discrepancy between experimental observations and predictions for crack propagation may be associated with relief in stress that initial cracking allows, but which remains unaccounted for in this analysis.

This study continues to support the contention that observations of cracking in cryoprotective agents can be rationalized on the basis of thermo-mechanical stresses. To the extent that the onset of fractures is a critical event in cryopreservation, indicating structural damage to the cryopreserved organ, the current study provides a credible tool to predict initiation of fractures. Additional work remains to determine models that faithfully capture deformation and fracture under conditions of low temperatures, as well as to determine associated material properties.

## Acknowledgment

This study has been supported in part by National Heart Lung and Blood Institute - NIH, grant number R01 HL069944.

## References

1. Fahy GM, Saur J, Williams JR. Physical Problems With The Vitrification Of Large Biological Systems. *Cryobiology* 1980;27:492–510. [PubMed: 2249453]

2. Fahy, GM. Biological Effects of Vitrification and Devitrification. In: Pegg, DE.; Karow, AM., Jr., editors. *The Biophysics of Organ Preservation*. Plenum Publishing Corp.; New York: 1987. p. 265-297.
3. Kroener C, Luyet BJ. Formation of Cracks During the Vitrification of Glycerol Solutions and Disappearance of the Cracks During Rewarming. *Biodynamica* 1966;10(201):47–52. [PubMed: 5971629]
4. Taylor, MJ.; Song, YC.; Brockbank, KGM. Vitrification in Tissue Preservation: New Developments. In: Fuller, BJ.; Lane, N.; Benson, EE., editors. *Life in the Frozen State*. CRC Press; New York: 2004. p. 603-641.
5. Rabin, Y.; Steif, PS.; Taylor, MJ.; Walsh, JR.; Baicu, B. Cryomacroscopy of Vitrification: Selected Experiments on DP6 and VS55. 2005.  
<http://www.me.cmu.edu/faculty1/rabin/CryomacroscopyImages01.html>
6. Rabin Y, Taylor MJ, Walsh JR, Baicu S, Steif PS. Cryomacroscopy of Vitrification, Part I: A Prototype and Experimental Observations on the Cocktails VS55 and DP6. *Cell Preservation Technology* 2005;3(3):169–183. [PubMed: 16721425]
7. Steif PS, Palastro M, Wen CR, Baicu S, Taylor MJ, Rabin Y. Cryomacroscopy of Vitrification, Part II: Experimental Observations and Analysis of Fracture Formation in Vitrified VS55 and DP6. *Cell Preservation Technology* 2005;3(3):184–200. [PubMed: 16900261]
8. Pegg DE, Wusteman MC, Boylan S. Fractures in Cryopreserved Elastic Arteries. *Cryobiology* 1997;34(2):183–192. [PubMed: 9130389]
9. Plitz J, Rabin Y, Walsh JR. The Effect of Thermal Expansion of Ingredients on the Cocktails VS55 and DP6. *Cell Preservation Technology* 2004;2(3):215–226.
10. Rabin Y, Taylor MJ, Wolmark N. Thermal Expansion Measurements of Frozen Biological Tissues at Cryogenic Temperatures. *ASME Journal of Biomechanical Engineering* 1998;120(2):259–266.
11. Rabin Y, Bell E. Thermal Expansion Measurements of Cryoprotective Agents, Part I: A New Experimental Apparatus. *Cryobiology* 2003;46:254–263. [PubMed: 12818215]
12. Rabin Y, Bell E. Thermal Expansion Measurements of Cryoprotective Agents, Part II: Measurements of DP6 and VS55, and Comparison with DMSO. *Cryobiology* 2003;46:264–270. [PubMed: 12818216]
13. Rabin Y, Plitz J. Thermal Expansion of Blood Vessels and Muscle Specimens Permeated with DMSO, DP6, and VS55 in Cryogenic Temperatures. *Annals of Biomedical Engineering* 2005;33(9):1213–1228. [PubMed: 16133928]
14. Rabin Y, Steif PS. Analysis of Thermo-Mechanical Stress During Cryopreservation of Blood Vessels. *Cryoletters* 2005;26(6):409–411. [PubMed: 16598896]
15. Song YC, Khirabadi BS, Lightfoot FG, Brockbank KGM, Taylor MJ. Vitreous Cryopreservation Maintains the Function of Vascular Grafts. *Nature Biotechnology* 2000;18:296–299.
16. Karow, AM. Biophysical and Chemical Considerations in Cryopreservation. In: Karow, AM.; Pegg, DE., editors. *Organ Preservation for Transplantation*. Dekker; New York: 1981. p. 113
17. Luyet BJ. The Vitrification of Organic Colloids and of Protoplasm. *Biodynamica* 1937;1(29):1–14.
18. Taylor, MJ. Sub-Zero Preservation and the Prospect of Long-Term Storage of Multicellular Tissues and Organs. In: Calne, RY., editor. *Transplantation Immunology: Clinical and Experimental*. Oxford University Press; Oxford, New York, Tokyo: 1984. p. 360-390.
19. Taylor, MJ. Physico-Chemical Principles of Low Temperature Biology. In: Grout, BW.; Morris, JG., editors. *The Effects of Low Temperatures on Biological System*. Edward Arnold; London: 1987. p. 3-71.
20. Rabin, Y.; Steif, PS. Advances in Heat and Mass Transfer in Biotechnology. IMECE 1999. Nashville, Tennessee: 1999. Thermal Stress Modeling of Freezing Biological Tissues; p. 183-188. ASME HTD-Vol. 363/BED-Vol. 44 (1999)
21. Rabin Y, Steif PS. Thermal Stress Modeling in Cryosurgery. *International Journal of Solids and Structures* 2000;37:2363–2375.
22. Rabin Y, Steif PS, Hess KC, Jimenez-Rios JL, Palastro MC. Fracture Formation in Vitrified Thin Films of Cryoprotectants. *Cryobiology* 2006;53(1):75–95. [PubMed: 16784737]
23. Rabin, Y.; Steif, PS.; Hess, KC.; Jimenez-Rios, JL. Cryomacroscopy of Fracture Formation in Vitrified Thin Films of Cryoprotectants. 2006.  
<http://www.me.cmu.edu/faculty1/rabin/CryomacroscopyImages02.html>



24. Malvern, LE. Introduction to the Mechanics of a Continuous Medium. Prentice-Hall; Englewood Cliffs, New Jersey: 1969.
25. Rabin Y. The Effect of Temperature-Dependent Thermophysical Properties in Heat Transfer Simulations of Biomaterials in Cryogenic Temperatures. *CryoLetters* 2000;21:163–170. [PubMed: 12148047]
26. Nieto-Draghi C, Avalos JB. Transport Properties of Dimethyl Sulfoxide Aqueous Solutions. *Journal of Chemical Physics* 2003;119(9):4782–4789.
27. Schichman SA, Amey RL. Viscosity and Local Liquid Structure in Dimethyl Sulfoxide - Water Mixtures. *J. of Phys. Chem* 1971;75(1):98–102.
28. Westh P. Thermal expansivity, molar volume, and heat capacity of liquid dimethyl sulfoxide-water mixtures at subzero temperatures. *Journal of Physical Chemistry* 1994;98(12):3222–3225.
29. Richerson, DW. *Modern Ceramic Engineering: Properties, Processing, and Use in Design*. Marcel Dekker, Inc.; New York: 1992.
30. Ashby, MF.; Jones, DRH. *Engineering Materials: An Introduction to their Properties and Applications*. Pergamon Press; Oxford: 1980.

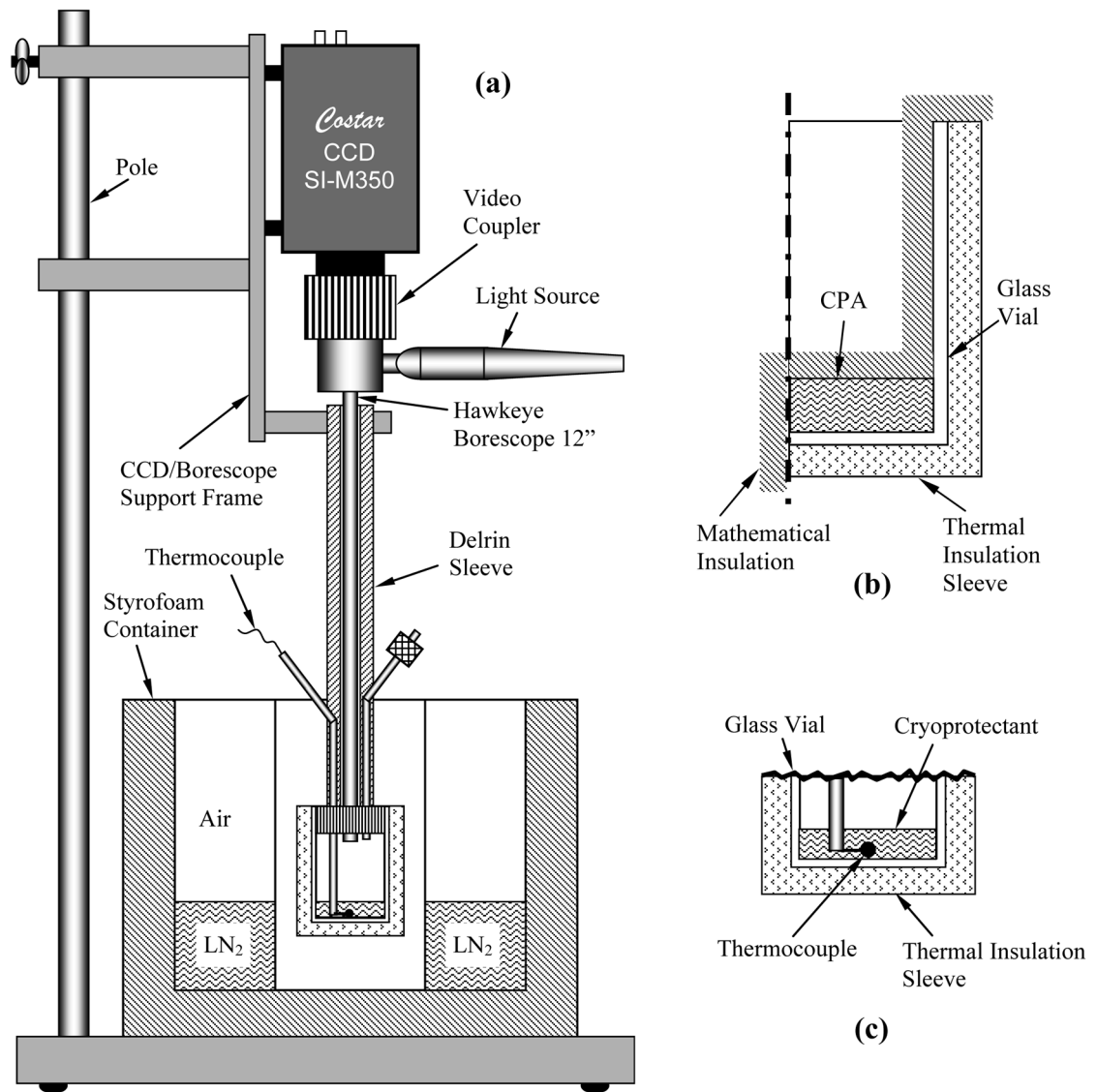


**Figure 1.** Schematic illustration of: (a) the macroscope set up [6], (b) the thermal stress problem analyzed in the current study, and (c) a closer view of the bottom of the vial, including the location of the thermocouple junction.

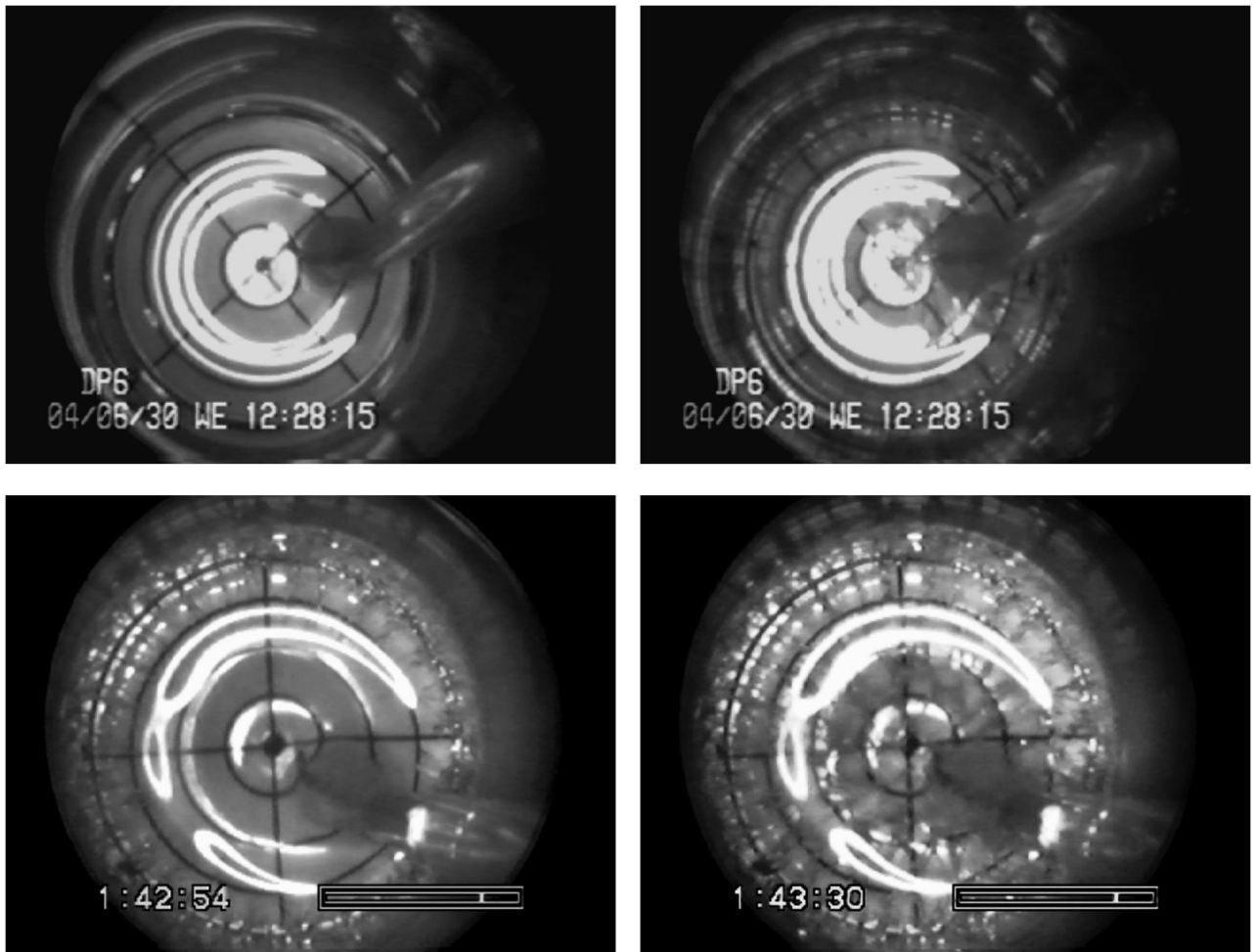


**Figure 2.**

Cracking in the CPA DP6, recorded with a cryomicroscope (Fig. 1), subject to slow cooling rate when the temperature at the center of the vial is  $-127.2^{\circ}\text{C}$  before (top-left) and after (top-right) cracking, and subject to a fast cooling rate when the temperature at the center of the vial is  $-129.8^{\circ}\text{C}$  (bottom-left) and  $-156.4^{\circ}\text{C}$  (bottom-right).

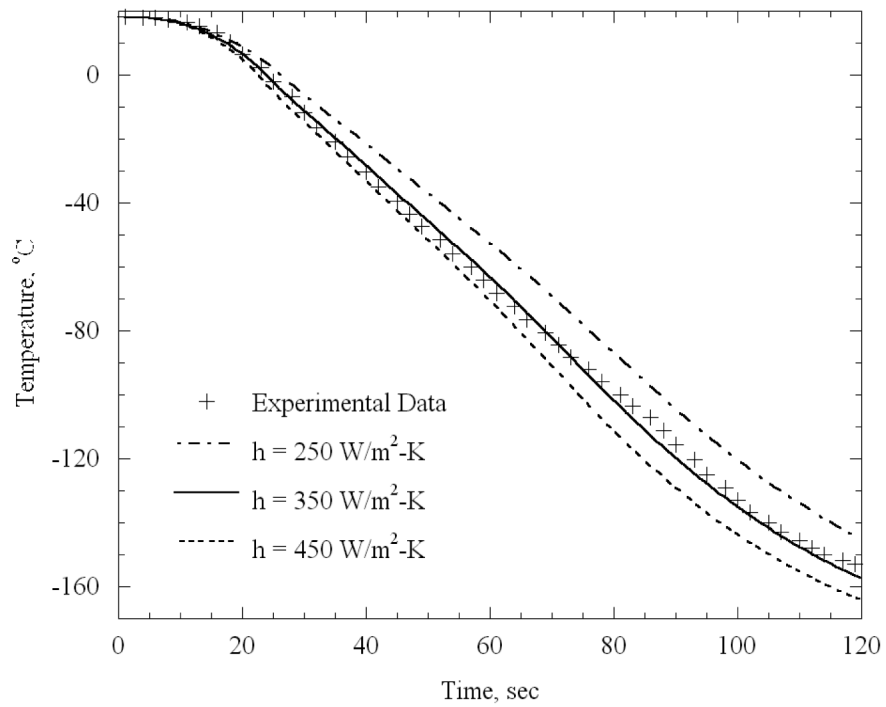


**Figure 3.** Best-fit results for the heat transfer coefficient by convection ( $350 \text{ W/m}^2\text{-K}$ ), for the fast cooling case. Temperature measurements are compared with simulation results at the geometric center of the CPA, using ANSYS and the thermophysical properties listed in Table 1. For reference, two additional cases are plotted using convection coefficient values of  $250$  and  $450 \text{ W/m}^2\text{-K}$ .

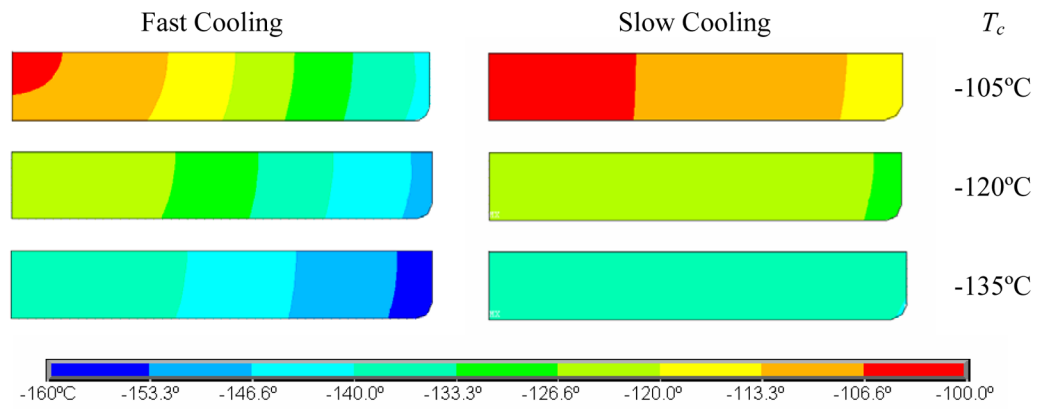


**Figure 4.** Simulated temperature distribution in the CPA for the fast (left column) and slow (right column) cooling rates, at three representative temperatures,  $T_c$ , at the geometrical center of the CPA.

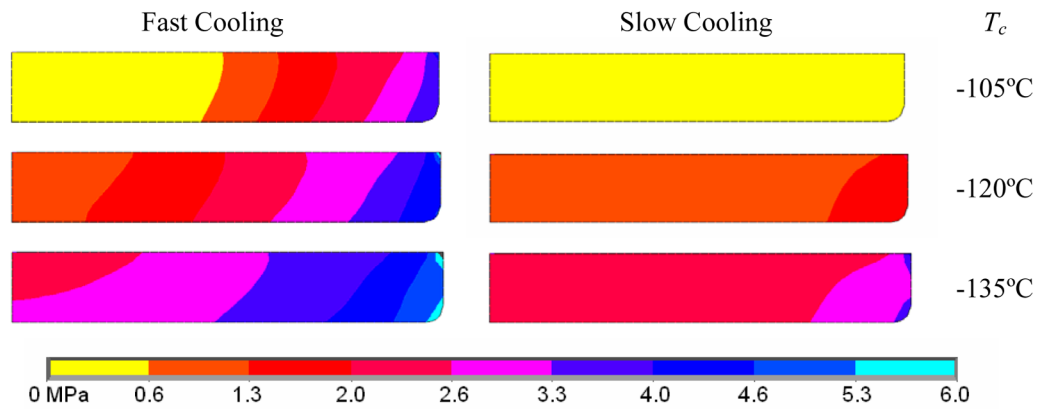


**Figure 5.**

Circumferential stress distribution in the CPA as predicted by ANSYS, for the cases of fast (left column) and slow (right column) cooling rates, at three representative temperatures,  $T_c$ , at the geometrical center of the CPA. These stress distributions correspond to the temperature distributions presented in Fig. 4.

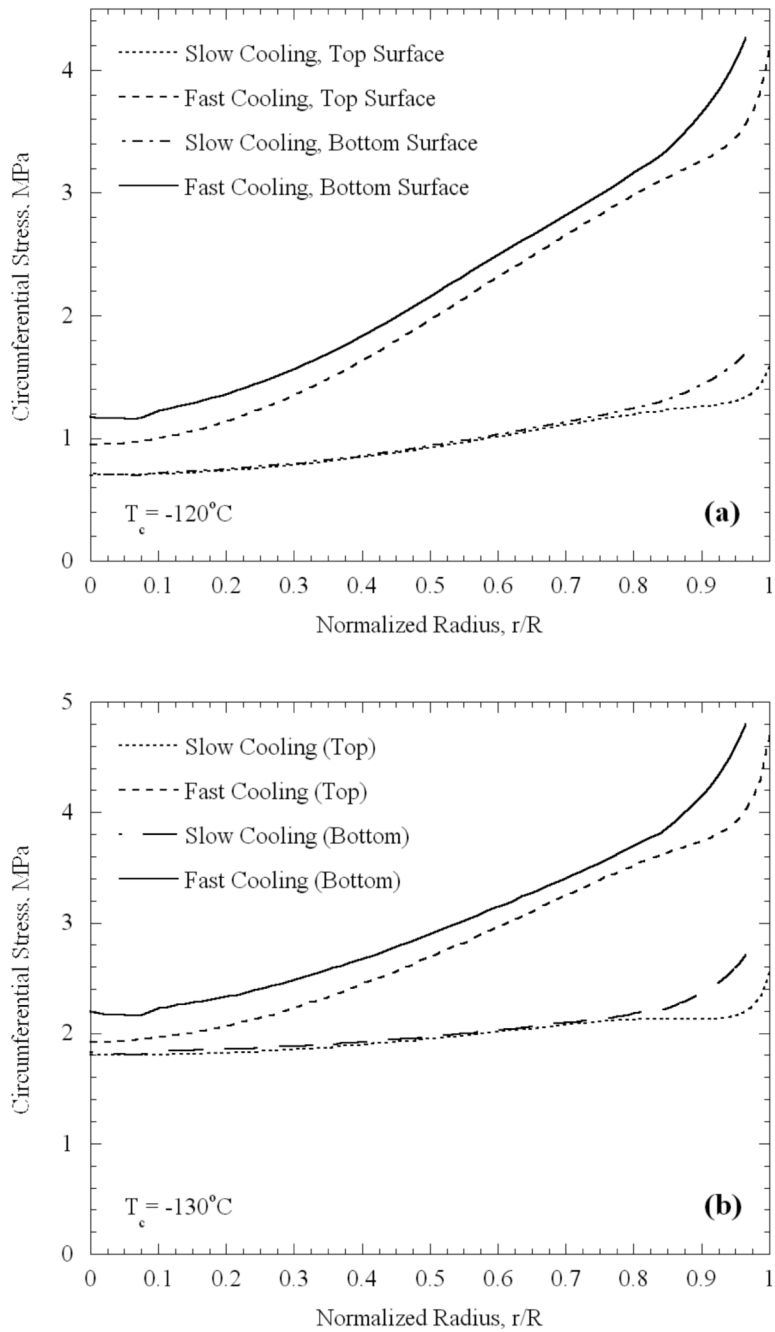


**Figure 6.** Circumferential stress distribution along the top and bottom surfaces of the CPA, when the center temperature,  $T_c$ , reaches a value of (a)  $-120^\circ\text{C}$ , and (b)  $-130^\circ\text{C}$ .

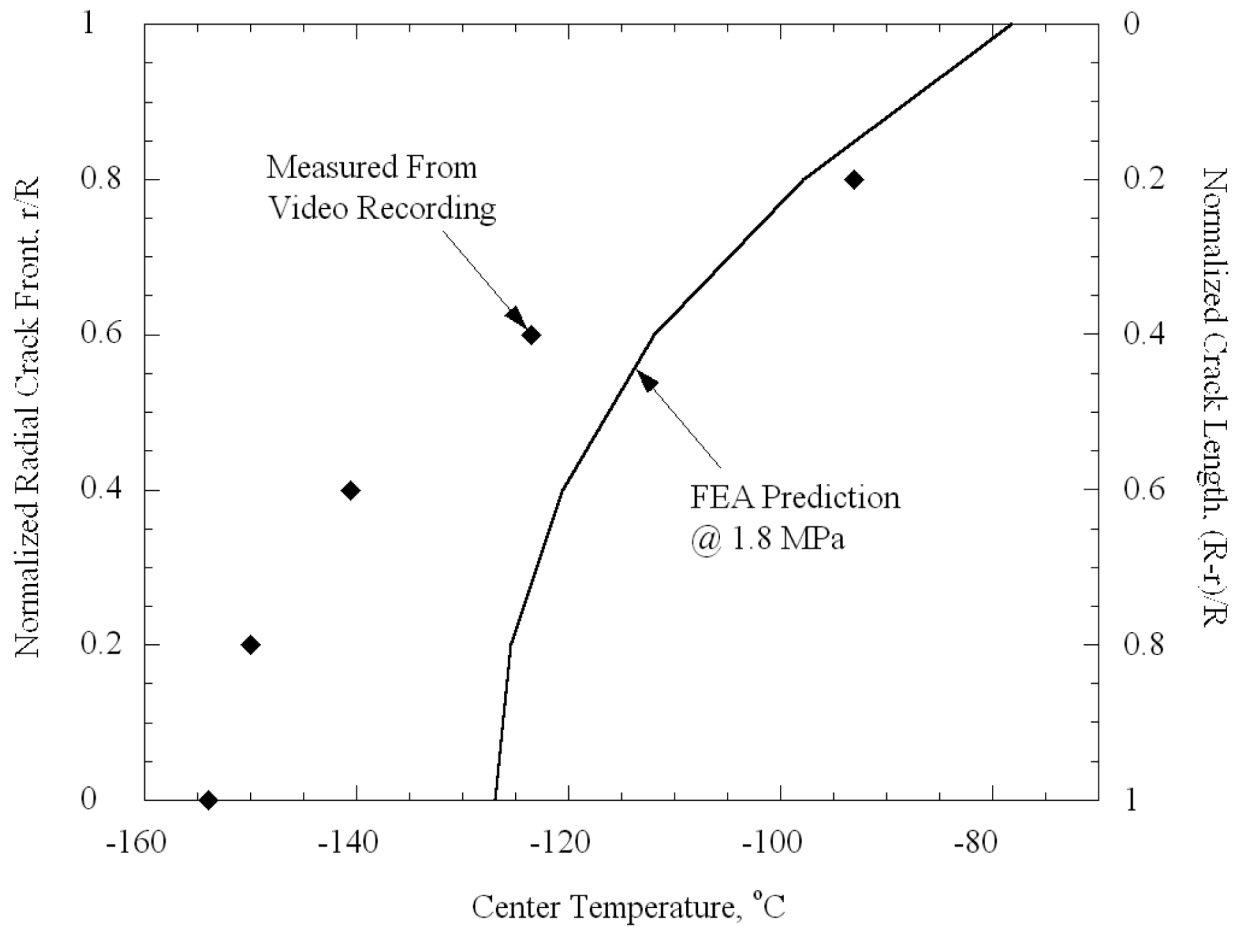


**Figure 7.** Predicted (solid curve) and observed (data points) crack front location in the CPA as a function of center-line temperature,  $T_c$ , for the case of fast cooling. Predicted location is based on finite element analysis and corresponds to tensile stress level of 1.8 MPa.



**Table 1**

Physical properties used in the current analysis

|   | Cryoprotectant   |                   | Glass | Delrin |
|---|--|-------------------|-------|--------|
| Thermal Conductivity, $k$ , W/m-K                         | $2135 T^{-1.235} - 1.893$  | $T < 273\text{K}$ | 0.78  | 0.35   |
| Density, $\rho$ , kg/m <sup>3</sup> ( $T$ in K)           | 0.2  | $273\text{K} < T$ | 2700  | 1420   |
| Specific Heat, $C_p$ , J/kg-K ( $T$ in K)                 | $3.9 \times 10^{-7} T^2 - 1.9 \times 10^{-5} T - 2.8 \times 10^{-2}$ |                   | 840   | 1470   |
| Thermal Expansion, $\beta \times 10^6$ , 1/°C ( $T$ in K) | $0.7798 T + 193.5$   |                   | 4     | N/A    |
| Poisson Ratio, $\nu$                                      | 0.2  |                   | 0.2   | N/A    |
| Elastic Modulus, $E$ , GPa                                | 1  |                   | 70    | N/A    |